CrossMark

Unravelling the energy transfer mechanism in bismuth co-activation of LaInO₃:Sm³⁺/Ho³⁺ nanophosphor for color-tunable luminescence†

Ch. Satya Kamal,[ac] T. K. Visweswara Rao,[ac] P. V. S. S. S. N. Reddy,[a] K. Sujatha,[a] Babajide Patrick Ajayi,[b] Jacek B. Jasinski[b] and K. Ramachandra Rao*[ab]

A series of single-phased and color tunable LaInO₃:Bi³⁺,Ho³⁺/Sm³⁺ nano phosphors were synthesized via a cost effective and low temperature chemical route. The crystal structure, morphology, photoluminescence (PL) and energy transfer mechanism between Bi³⁺ to Ho³⁺/Sm³⁺ were investigated in detail. The considerable spectral overlap between the broad emission band of Bi³⁺ around 400–500 nm and the excitation band of Ho³⁺ and Sm³⁺ supports the efficient energy transfer from Bi³⁺ to Ho³⁺/Sm³⁺, which enhances the PL intensity remarkably. The energy transfer efficiency between Bi³⁺ and Ho³⁺/Sm³⁺ in LaInO₃ was also calculated and the efficiency increased linearly with increasing concentration of Ho³⁺ and Sm³⁺. The emission hue can be tuned from blue to green and pink by varying the content of Ho³⁺/Sm³⁺. This investigation will extend an understanding of interactions between Bi³⁺ and rare earth ions in semiconducting host LaInO₃ and show the potential applications of Bi³⁺, Ho³⁺/Sm³⁺ co-doped nanophosphors in displays and light emitting diodes.

Introduction

Owing to the gradual increase in energy consumption, light emitting diodes, as fourth generation lighting source, have been used widely in general illumination purposes and for display applications on account of their excellent characteristics. The manufacture of LEDs using inorganic phosphors or single-phase emitting phosphors excited by ultraviolet (UV) chips has received great attention. The single-phase phosphor-converted UV LEDs and phosphors with excellent red and green emission properties have become a vital part in the field of back lighting display applications. In the view of the above-mentioned reasons, research on rare earth (RE) activated luminescence materials plays a major technological role in lighting applications. Indeed, the absorption cross section of RE ions is small because of the parity forbidden character of 4f–4f transitions, and consequently RE ions cannot be excited directly by illuminating light.[1–8] Therefore, to improve the efficiencies and luminescence properties of RE ions, several

methods are chosen, such as host absorption, f–d absorption, charge transfer state absorption, and energy transfer (ET).

Rare earth (RE) and transition ion-doped aluminates and gallates have been studied extensively for their display applications.[9–14] SrAl₂O₄:Dy³⁺,Eu²⁺ has been regarded to deliver a good green long persisting phosphorescence.[15] Furthermore, indates, being used as the host lattice for luminescence and being doped with rare-earth ions were also reported.[15–19] A few rare-earth doped LaInO₃ phosphors have been reported as an alternative luminescence material because of their high thermal and chemical stability. Silicon coated core–shell structured LaInO₃:Sm³⁺,Tb³⁺ phosphors have been used for their diverse luminescent properties.[20–23] Despite their use as a photoluminescent host, the energy transfer mechanism between sensitizer and activator is still unclear.

The semiconducting compound, LaInO₃, with a bandgap of 3.2 eV, belongs to the orthorhombically distorted perovskite-like structure with the space group Pnma[24] and is found to be a potential candidate for several applications in various fields, such as oxygen sensing,[25] solid oxide fuel cells (SOFC) and the presence of In³⁺ in the host lattice enhances its electrical conductivity, which can be used for display applications.[26] Semiconducting oxide-based phosphors like LaInO₃ are promising candidates with sufficient conductivity to overcome the charge build-up on the phosphor surfaces, in addition to their thermal and chemical stability.[27,28] L. I. van Steensel et al. showed that LaInO₃:Bi³⁺ is an efficient, blue-emitting photo luminescent material[29] and researchers have reported that on co-doping with Bi³⁺, it acts as an excellent sensitizer to enhance

aCrystal Growth and Nano-Science Research Center, Department of Physics, Government College (A), Rajamahendravaram, Andhra Pradesh, India-533105. E-mail: drkrcr@gmail.com

bConn Center for Renewable Energy Research, University of Louisville, KY, USA

cDepartment of Physics, Adikavi Nannaya University, Rajamahendravaram, Andhra Pradesh, India

phosphor materials. The XRD patterns of pure LaInO$_3$ calcined at three different temperatures (700 °C, 900 °C, 1000 °C) is shown in ESI Fig. 1a,† indicating that LaInO$_3$ began to crystallize at 700 °C. All the diffraction peaks of the doped and co-doped LaInO$_3$ samples annealed at 1000 °C are in agreement with the previously reported data,[26,45] indicating that the obtained samples are in a pure orthorhombic phase, where no impurity phase is detected, indicating that the dopants dissolved completely in the LaInO$_3$ host lattice.

In addition, it can be observed from ESI Fig. 1b† that the diffraction peak positions are shifted slightly to a higher angle, when Bi^{3+} or Bi^{3+}, Ho^{3+}/Sm^{3+} ions were doped into the LaInO$_3$ host, which can be due to the replacement of larger-size La^{3+} (1.16 Å) sites by the smaller-size trivalent Ho^{3+}, Sm^{3+} and Bi^{3+} ions (1.051 Å, 1.08 Å, and 1.03 Å), leading to lattice distortion, consequently contracting the lattice parameters, as illustrated in ESI Table S1.† The three-dimensional structure diagram shows the crystal structure of LaInO$_3$, the blue octahedrons represent the InO$_6$ units, whereas La^{3+} is in the center of the eight InO$_6$ octahedrons; hence, rare earth dopants Ho^{3+} or Sm^{3+} and Bi^{3+} will be replacing La^{3+} in the LaInO$_3$ structure. The crystallite size of all the samples was calculated from the Scherrer equation $D = 0.9\lambda/\beta \cos \theta$, where D is the average particles size, λ is the wavelength of X-rays and β is the corrected full width at half maximum (FWHM) of an observed peak.[46] The average crystallite size (D) of pure LaInO$_3$, doped and co-doped LaInO$_3$ particles, which are annealed at 1000 °C, were estimated to be around 35 nm.

SEM with energy dispersive X-ray analysis

Fig. 2a and b shows the Scanning Electron Microscopy (SEM) images of LaInO$_3$:(3 at%)Bi^{3+},(1 at%)Ho^{3+}, and LaInO$_3$:(3 at%) Bi^{3+},(2 at%)Sm^{3+} samples. Crystallization granules and agglomeration of particles were observed in the present phosphors. ESI Fig. 2a and b† shows an SEM image of pure LaInO$_3$, indicating irregular spherical particles with a size between 20 and 70 nm. This may be due to agglomeration among the phosphor particles during calcination. Compared to the Bi^{3+} single-doped sample, the Bi^{3+}, Ho^{3+}/Sm^{3+} co-doped phosphors have a smaller particle size distribution. Hence, the effect of coalescence could be decreased by single and co-doping in the host. The decrease in particle size is also explained as follows:

In poly synthesis, ethylene glycol acts as the capping agent for covering the nanoparticles and controlling the agglomeration. On the other hand, during annealing at 1000 °C, the ligand evaporates and nanoparticles due to high surface energy form a neck by solid state diffusion process, which leads to agglomeration and particle growth. The differences in ionic radii between La^{3+} and Bi^{3+}, Ho^{3+}, and Sm^{3+} ions lead to a lattice distortion, which encourages a decrease in particle size. Hence, crystallite and particle size reduces by co-doping due to a grain growth inhibition effect. Energy dispersive X-ray spectroscopy (EDS) was used to determine the composition of the samples and it shows good agreement with the nominal sample composition. (Refer to the inset of Fig. 3a and b.)
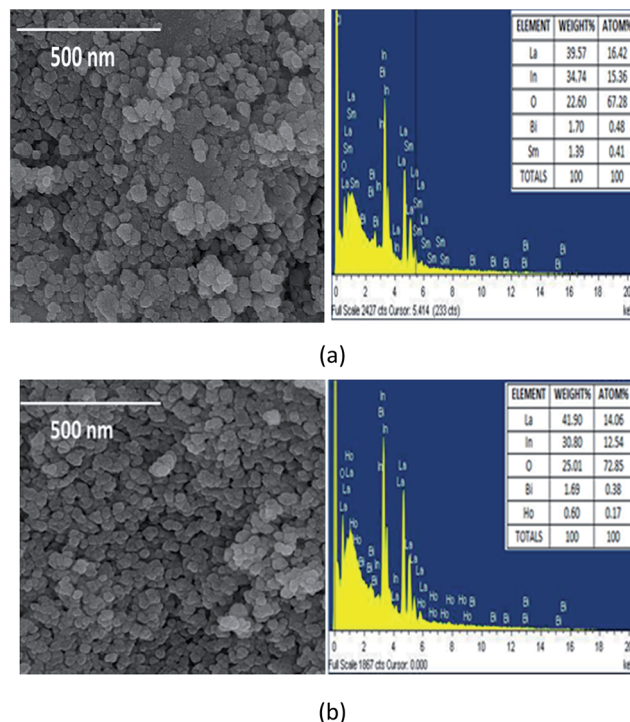

Fig. 2 (a and b) SEM images and EDAX spectra's of (a) Bi^{3+}, Ho^{3+} and (b) Bi^{3+}, Sm^{3+} doped LaInO$_3$.
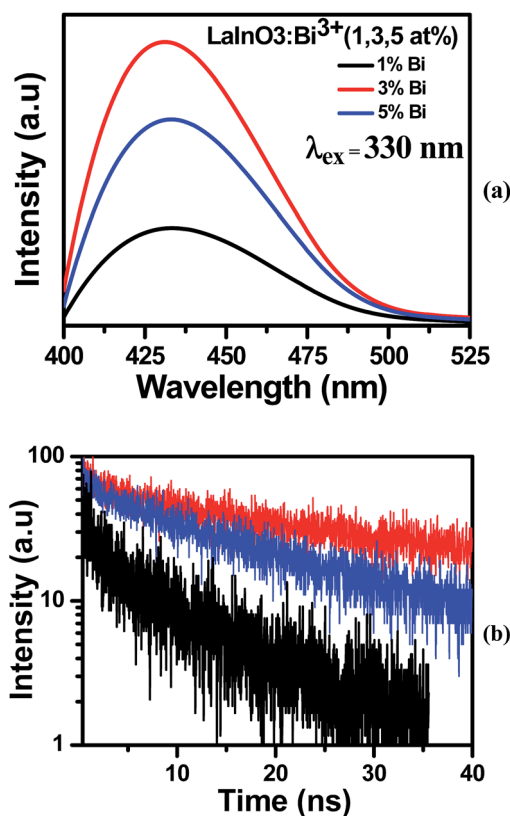

Fig. 3 (a and b) Emission and decay curves of the LaInO$_3$:Bi^{3+}(1, 3, 5 at%) samples heat at 1000 °C.

Photoluminescence and energy transfer mechanism

The emission and decay spectra of LaInO$_3$:Bi^{3+}(1, 3, and 5 at%) samples heated to 1000 °C are given in Fig. 3a and b respectively. From Fig. 3a, it can be observed that all samples have broad emission band centered at 432 nm, which can be attributed to the $^3P_1$–$^1S_0$ transition of Bi^{3+} ions upon excitation with 330 nm.[29] With increasing Bi^{3+} concentration, the intensity of the 432 nm emission band increases and reaches a maximum at 3 at% and then decreases remarkably when the Bi^{3+} content is increased further, which is due to concentration quenching. This is also confirmed by corresponding average bi-exponential life time value (295, 329, 273 ns) of decay curves shown in Fig. 3(b). In the excitation spectra (ESI Fig. 3†), a broad excitation band ranging from 300 to 350 nm with a maximum at about 330 nm was observed, arising from $^1S_0$–$^3P_1$ transition of Bi^{3+}.

The overlap spectra of the emission and allowed absorption create interest on the effective radiative energy transfer (ET) mechanism. Fig. 4 presents the excitation spectra of LaInO$_3$:Sm^{3+}(2 at%) LaInO$_3$:Ho^{3+}(1 at%) and emission spectra of LaInO$_3$:Bi^{3+}(3 at%) samples. The appearance of the excitation bands of Ho^{3+} and Sm^{3+} was clearly visible in the emission bands of Bi^{3+}. Therefore, it is expected that efficient energy transfer can occur from Bi^{3+} to Ho^{3+}/Sm^{3+}.

The excitation spectra of the Bi^{3+}, Ho^{3+}/Sm^{3+}-doped samples monitored at rare earth (RE) emission lines (544 nm and 603 nm) exhibited a broad excitation band arising from the $^1S_0$–$^3P_1$ transition of Bi^{3+} in the wavelength range of 300–350 nm, accompanying the Ho^{3+}/Sm^{3+} excitation lines. The same is shown in Fig. 5a–d, which represents the excitation and emission spectra of LaInO$_3$:3at%Bi^{3+},(0.5, 1, 1.5 at%)Ho^{3+} and LaInO$_3$:3at%Bi^{3+},(1, 1.5, 2, 2.5 at%)Sm^{3+} samples.

Under 330 nm and 333 nm excitation wavelengths, the samples consist of both blue-green emissions from Bi^{3+} and strong green emissions from Ho^{3+} and orange red emission from Sm^{3+}. By keeping Bi^{3+} at 3 at% and varying the Ho^{3+} and Sm^{3+} content, the intensity of Bi^{3+} emission decreases monotonously, whereas the intensity of Ho^{3+}/Sm^{3+} emission increases gradually and reaches a maximum at Ho^{3+} (1 at%) and Sm^{3+}

Fig. 4 Spectral overlap of excitation spectra of LaInO$_3$:Sm^{3+}(2 at%), LaInO$_3$:Ho^{3+}(1 at%) and emission spectra of LaInO$_3$:Bi^{3+}(3 at%) samples heated at 1000 °C.

(2 at%), and the Ho^{3+} and Sm^{3+} emissions then decrease with further increase in concentration, which can be rationalized as concentration quenching. The changes in emission intensity of Bi^{3+} as a function of Sm^{3+} and Ho^{3+} concentrations is clearly demonstrated in Fig. 5e–f. All abovementioned processes show that the emissions of Ho^{3+} and Sm^{3+} actually come from the ET process from Bi^{3+} to Ho^{3+}/Sm^{3+} ions. To investigate the effect of Bi^{3+} doping in enhancing the PL intensity, single doped Ho^{3+}/Sm^{3+}:LaInO$_3$ emission spectra are shown in ESI Fig. 4.† In addition, to support this ET process, the decay curves of all samples were measured, as shown in Fig. 6. For all samples, bi exponential luminescence decay curves were obtained and the lifetimes were characterized using the average lifetime (τ). The luminescence decay times (τ) of Bi^{3+} were obtained at 260, 228 and 192 ns for LaInO$_3$:Bi^{3+}(3 at%),Ho^{3+}(0.5, 1, 1.5 at%) and for LaInO$_3$:Bi^{3+}(3 at%),Sm^{3+}(1, 1.5, 2, 2.5 at%) 303, 291 and 211, 182 ns and also the corresponding decay times of Ho^{3+} 149, 179, and 122 µs, Sm^{3+} 1.22, 1.42, 1.73 and 1.13 ms, respectively. The increase in Ho^{3+}/Sm^{3+} content leads to the faster decay of Bi^{3+} emission, which was attributed to ET from Bi^{3+} to Ho^{3+}/Sm^{3+}. The corresponding energy level diagram of LaInO$_3$:Bi^{3+},Ho^{3+} and LaInO$_3$:Bi^{3+},Sm^{3+} with optical transitions and energy transfer process are displayed in Fig. 7. In this process, when excited by UV energy, the electrons of Bi^{3+} ions absorb energy and jump from the ground state $^1S_0$ to a higher level excited state $^3P_1$; the excited electrons then relax to the lower energy level (the bottom of parabola) by non-radiative relaxation. Hence, from the lower energy level of $^3P_1$, energy can be transferred to the $^4K_{11/2}$ level of Sm^{3+} and $^5F_1$ level of Ho^{3+} via an ET process (Cross relaxation) between these levels. Therefore, by co-doping with Bi^{3+} ions might improve the emission intensity of Sm^{3+} and Ho^{3+}. Finally, a part of the electrons of Bi^{3+} ions may radiate back to the ground state by emitting blue emission and can be reabsorbed by the ground state levels of Sm^{3+} and Ho^{3+} i.e. $^6H_{5/2}$ and $^5I_8$, which also leads to energy transfer (because spectral overlap is observed in both Sm^{3+} and Ho^{3+}), and can be subsequently excited to the respective high level excited state. The excited electrons relax to the $^5F_4$, $^5S_2$ level of Ho^{3+} and the $^4G_{5/2}$ level of Sm^{3+} by non-radiative transition, and finally electrons return to the ground states of Ho^{3+} and Sm^{3+} ions by emitting green and pink lines, respectively.

The ET efficiency η_T of Bi^{3+}–Ho^{3+} and Bi^{3+}–Sm^{3+} can be calculated using the following eqn (1)[35,36]

$$\eta_T = 1 - \frac{\tau_s}{\tau_{s_0}} \qquad (1)$$

where τ_s and τ_{s_0} represent the life time values of the sensitizer Bi^{3+} in the presence and absence of Ho^{3+} and Sm^{3+}. The energy-transfer efficiency η_T values from Bi^{3+} to Sm^{3+} to Ho^{3+} for LaInO$_3$ are listed in Table 1. Generally, the ET mechanism consists of two main aspects;[39] one is exchange interaction and the other is an electric multipolar interaction. The exchange interaction from Bi^{3+} prevails when $R_c > R$ and an electric multipolar interaction from Bi^{3+} to Ho^{3+}/Sm^{3+} dominates when $R_c < R$. In this case, the critical distance (R) for the activators is restricted in the range of 5–8 Å.[47] When the value reaches the critical transfer distance, the electric multipolar interaction will take place.
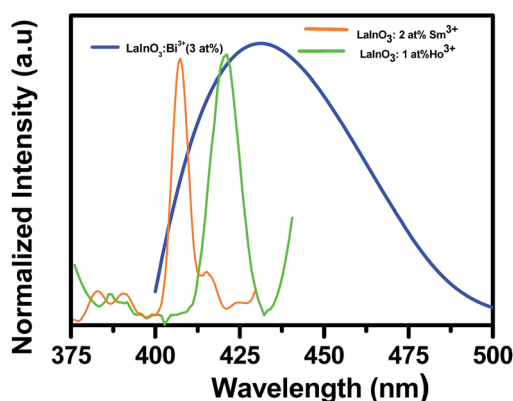
Fig. 5 Excitation and emission spectra of LaInO₃:3at%Bi³⁺,(0.5, 1, 1.5 at%)Ho³⁺ (a and b) and LaInO₃:3at%Bi³⁺,(1, 1.5, 2, 2.5 at%)Sm³⁺ (c and d) heated at 1000 °C. Variations in the emission intensity for Sm³⁺/Ho³⁺ and Bi³⁺ with different (e) Sm³⁺/Ho³⁺ (f) concentrations.

The critical distance R_c between Bi³⁺ and Ho³⁺/Sm³⁺ in the LaInO₃ host can be estimated by the following equation:[48]

$$R_c \approx 2\left(\frac{3V}{4\pi \chi_c Z}\right)^{1/3} \quad (2)$$

where V is the volume of the unit cell, X_c is the total critical concentration of dopant ions, and Z represents the number of activator ions in the unit cell. Using the parameters of the LaInO₃ host ($V = 289.63$ Å, $Z = 2$) and the estimated critical

concentration of dopant ions (Bi³⁺–Ho³⁺) ($X_c = 0.04$) and (Bi³⁺–Sm³⁺) ($X_c = 0.05$), the critical distance $R_{Bi–Ho/Sm}$ was calculated to be 11.99 Å and 11.14 Å. This value is much larger than 5 Å, suggesting the low probability of exchange interaction for energy transfer. Therefore, it is reliable to consider that the multipolar interaction is dominant for energy transfer from Bi³⁺ to Ho³⁺/Sm³⁺ in LaInO₃.

To study the effect of the Ho³⁺/Sm³⁺ ions doping content on the color of LaInO₃:3at%Bi³⁺, we synthesized a series of samples

Fig. 6 Decay curves of Bi^{3+} (a and b) and Ho^{3+}, Sm^{3+} (c and d) in LaInO$_3$:3at%Bi^{3+},(0.5, 1, 1.5 at%)Ho^{3+} and LaInO$_3$:3at%Bi^{3+},(1, 1.5, 2, 2.5 at%)Sm^{3+}.

with the chemical compositions of LaInO$_3$:3at%Bi^{3+},Ho^{3+}(0.5, 1, 1.5 at%)/Sm^{3+}(1, 1.5, 2, 2.5 at%). The Commission International de L'Eclairage (CIE) chromaticity coordinates of the single-phased emission-tunable phosphors are presented in Fig. 8.

The CIE chromaticity coordinates of pure 3 at% Bi^{3+}, 3 at% Bi^{3+}, 1 at% Ho^{3+} and 3 at% Bi^{3+}, 2 at% Sm^{3+} activated LaInO$_3$ phosphors were (0.15, 0.03), (0.21, 0.25), and (0.33, 0.17)

Table 1 ET efficiency (RE^{3+}) of the phosphors

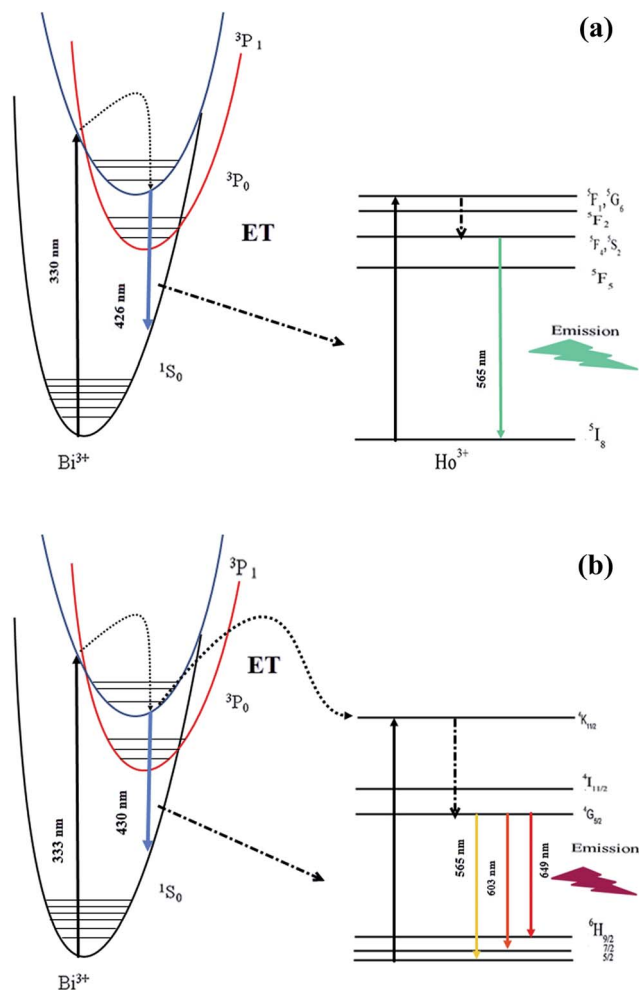| Phosphors	Concentration (x)	Efficiency η_{ET} (%)
LaInO$_3$:3at%Bi^{3+},xHo^{3+}	0.5	39
	1.0	42
	1.5	59
LaInO$_3$:3at%Bi^{3+},xSm^{3+}	1.0	0.8
	1.5	12
	2.0	36
	2.5	45

Fig. 7 Energy level diagram and ET schemes of LaInO$_3$:Bi^{3+},Ho^{3+} (a) Sm^{3+} (b).

Fig. 8 CIE chromaticity diagram of the (point a) LaInO$_3$:3at%Bi^{3+}, (points b–d) LaInO$_3$:3at%Bi^{3+},(0.5, 1, 1.5 at%)Ho^{3+} and (points e–h) LaInO$_3$:3at%Bi^{3+},(1, 1.5, 2, 2.5 at%)Sm^{3+} phosphors.

respectively. From the CIE diagram, it can be seen that the CIE chromaticity coordinates move from the bright blue to blue-green region and pink region as the amount of Ho^{3+}/Sm^{3+} varies, indicating that the developed phosphor may potentially be used as a single phase phosphor for UV light-emitting diodes and field display applications.

Conclusion

We synthesized a series of single phased and color-tunable $LaInO_3:3at\%Bi^{3+}$, $LaInO_3:3at\%Bi^{3+}$,$Ho^{3+}(0.5, 1, 1.5$ at%)/$Sm^{3+}(1, 1.5, 2, 2.5$ at%) nanophosphors using the polyol method, and all the dopants were incorporated into the $LaInO_3$ lattice, as determined via the XRD patterns. The photoluminescence properties, life time studies and energy transfer process were investigated in detail. The energy transfer from Bi^{3+} to Ho^{3+}/Sm^{3+} and the energy transfer efficiency of $LaInO_3:3at\%Bi^{3+}$,Ho^{3+} and $LaInO_3:3at\%Bi^{3+}$,Sm^{3+} samples, which were calculated from the PL and decay curves, were 59 and 45%, respectively. Furthermore, the CIE diagram showed that the colors can be tuned from bright blue to blue-green and pink, indicating that the developed phosphor may potentially be used as a single phase phosphor for UV light-emitting diodes, VFD, FED, and other photoelectric fields.

Acknowledgements

Notes and references

1 G. Blasse and B. Grabmaier, *Luminescent materials*, Springer Science & Business Media, 2012.
2 E. F. Schubert and J. K. Kim, *Science*, 2005, **308**, 1274–1278.
3 R. Wei, C. Ma, Y. Wei, J. Gao and H. Guo, *Opt. Express*, 2012, **20**, 29743–29750.
4 H. Guo, R. Wei and X. Liu, *Opt. Lett.*, 2012, **37**, 1670–1672.
5 W.-R. Liu, C. C. Lin, Y.-C. Chiu, Y.-T. Yeh, S.-M. Jang and R.-S. Liu, *Opt. Express*, 2010, **18**, 2946–2951.
6 A. Kuznetsov, A. Nikitin, V. Tikhomirov, M. Shestakov and V. Moshchalkov, *Appl. Phys. Lett.*, 2013, **102**, 161916.
7 S. Nigam, C. S. Kamal, K. R. Rao, V. Sudarsan and R. K. Vatsa, *J. Lumin.*, 2016, **178**, 219–225.
8 F. Wang, R. Deng, J. Wang, Q. Wang, Y. Han, H. Zhu, X. Chen and X. Liu, *Nat. Mater.*, 2011, **10**, 968–973.
9 A. Baszczuk, M. Jasiorski, M. Nyk, J. Hanuza, M. Mączka and W. Stręk, *J. Alloys Compd.*, 2005, **394**, 88–92.
10 Q. Shi, C. Wang, D. Zhang, S. Li, L. Zhang, W. Wang and J. Zhang, *Thin Solid Films*, 2012, **520**, 6845–6849.
11 C. S. Kamal, R. Mishra, D. K. Patel, K. R. Rao, V. Sudarsan and R. Vatsa, *Mater. Res. Bull.*, 2016, **81**, 127–133.
12 M. Yu, J. Lin, Y. Zhou and S. Wang, *Mater. Lett.*, 2002, **56**, 1007–1013.
13 X. Liu and J. Lin, *J. Appl. Phys.*, 2006, **100**, 124306.

14 T. Samuel, C. S. Kamal, K. Sujatha, V. Veeraiah, Y. Ramakrishana and K. R. Rao, *Optik*, 2016, **127**, 10575–10587.
15 X. Liu, R. Pang, Z. Quan, J. Yang and J. Lin, *J. Electrochem. Soc.*, 2007, **154**, J185–J189.
16 X. Liu and J. Lin, *J. Mater. Chem.*, 2008, **18**, 221–228.
17 X. Liu, C. Lin and J. Lin, *Appl. Phys. Lett.*, 2007, **90**, 081904.
18 X. Liu, C. Li, Z. Quan, Z. Cheng and J. Lin, *J. Phys. Chem. C*, 2007, **111**, 16601–16607.
19 X. Liu, C. Lin, Y. Luo and J. Lin, *J. Electrochem. Soc.*, 2007, **154**, J21–J27.
20 S. K. Chaluvadi, V. Aswin, P. Kumar, P. Singh, D. Haranath, P. K. Rout and A. Dogra, *J. Lumin.*, 2015, **166**, 244–247.
21 X. Liu, L. Yan and J. Lin, *J. Electrochem. Soc.*, 2009, **156**, P1–P6.
22 X. Liu and J. Lin, *Solid State Sci.*, 2009, **11**, 2030–2036.
23 Y. Shang, P. Yang, W. Wang, Y. Wang, N. Niu, S. Gai and J. Lin, *J. Alloys Compd.*, 2011, **509**, 837–844.
24 D. Rogers, J. Honig and J. Goodenough, *Mater. Res. Bull.*, 1967, **2**, 223–230.
25 V. Thangadurai and W. Weppner, *J. Electrochem. Soc.*, 2001, **148**, A1294–A1301.
26 H. He, X. Huang and L. Chen, *Solid State Ionics*, 2000, **130**, 183–193.
27 H. He, X. Huang and L. Chen, *Electrochim. Acta*, 2001, **46**, 2871–2877.
28 K. Sood, K. Singh and O. Pandey, *Trans. Indian Ceram. Soc.*, 2013, **72**, 32–35.
29 L. I. van Steensel, S. G. Bokhove, A. M. van de Craats, J. de Blank and G. Blasse, *Mater. Res. Bull.*, 1995, **30**, 1359–1362.
30 F. Angiuli, E. Cavalli and A. Belletti, *J. Solid State Chem.*, 2012, **192**, 289–295.
31 D. Chen, Y. Yu, P. Huang, H. Lin, Z. Shan, L. Zeng, A. Yang and Y. Wang, *Phys. Chem. Chem. Phys.*, 2010, **12**, 7775–7778.
32 Y. Zhydachevskii, L. Lipińska, M. Baran, M. Berkowski, A. Suchocki and A. Reszka, *Mater. Chem. Phys.*, 2014, **143**, 622–628.
33 E. Cavalli, F. Angiuli, A. Belletti and P. Boutinaud, *Opt. Mater.*, 2014, **36**, 1642–1648.
34 Z. Xia, D. Chen, M. Yang and T. Ying, *J. Phys. Chem. Solids*, 2010, **71**, 175–180.
35 L. Han, Y. Wang, J. Zhang and Y. Wang, *Mater. Chem. Phys.*, 2013, **139**, 87–91.
36 L. Chen, K.-J. Chen, S.-F. Hu and R.-S. Liu, *J. Mater. Chem.*, 2011, **21**, 3677–3685.
37 X. Wei, Y. Chen, X. Cheng, M. Yin and W. Xu, *Appl. Phys. B: Lasers Opt.*, 2010, **99**, 763–768.
38 H. Hara, S. Takeshita, T. Isobe, T. Sawayama and S. Niikura, *Mater. Sci. Eng., B*, 2013, **178**, 311–315.
39 P. Boutinaud, *Inorg. Chem.*, 2013, **52**, 6028–6038.
40 L. Wang, Z. Lv, W. Kang, X. Shangguan, J. Shi and Z. Hao, *Appl. Phys. Lett.*, 2013, **102**, 151909.
41 L. Wang, Q. Sun, Q. Liu and J. Shi, *J. Solid State Chem.*, 2012, **191**, 142–146.
42 H. Ju, W. Deng, B. Wang, J. Liu, X. Tao and S. Xu, *J. Alloys Compd.*, 2012, **516**, 153–156.

43 Y. Zhang, Z. Zhu, W. Zhang and Y. Qiao, *J. Alloys Compd.*, 2013, **566**, 164–167.

44 H. H. T. Vu, T. S. Atabaev, H.-K. Kim and Y.-H. Hwang, *J. Nanosci. Nanotechnol.*, 2012, **12**, 5847–5851.

45 E. Ruiz-Trejo, G. Tavizon and A. Arroyo-Landeros, *J. Phys. Chem. Solids*, 2003, **64**, 515–521.

46 C. Hu, Z. Zhang, H. Liu, P. Gao and Z. L. Wang, *Nanotechnology*, 2006, **17**, 5983.

47 H. He, R. Fu, Y. Cao, X. Song, Z. Pan, X. Zhao, Q. Xiao and R. Li, *Opt. Mater.*, 2010, **32**(5), 632–636.

48 G. Blasse, *Philips Res. Rep.*, 1969, **24**(2), 131–144.